Estimation and Filtering Techniques for High-Accuracy GPS Applications

S. M. Lichten
Tracking Systems and Applications Section

Techniques for determination of very precise orbits for satellites of the Global Positioning System (GPS) are currently being studied and demonstrated. These techniques can be used to make cm-accurate measurements of station locations relative to the geocenter, monitor earth orientation over timescales of hours, and provide tropospheric and clock delay calibrations during observations made with deep space radio antennas at sites where the GPS receivers have been collocated. For high-earth orbiters, meter-level knowledge of position will be available from GPS, while at low altitudes, sub-decimeter accuracy will be possible. Estimation of satellite orbits and other parameters such as ground station positions is carried out with a multi-satellite batch sequential pseudo-epoch state process noise filter. Both square-root information filtering (SRIF) and UD-factorized covariance filtering formulations are implemented in the software. A Bierman-modified Rauch-Tung-Striebal (BRTS) smoother runs in conjunction with the SRIF and UD filters to compute smoothed estimates and covariances. The filtering algorithms have been arranged to take advantage of sparse matrices and other characteristics of the GPS measurement scenarios. The filter includes unique error evaluation capabilities to assess effects from mismodeling. Process noise plays a key role in the orbit determination for stochastic behavior of transmitter/receiver clocks, atmosphere-induced delay fluctuations, and unmodeled satellite accelerations. The efficiency and accuracy of the SRIF and UD filter formulations are compared for GPS processing under a variety of conditions. With data from recent GPS experiments using the seven satellites currently in orbit, continental ground baselines have been measured with GPS and with VLBI which agree to within 2.5 cm over distances of 2000 km, corresponding to a relative baseline accuracy of better than 1.5 parts in 10^8.

I. Introduction

The Global Positioning System (GPS) will consist of at least 21 satellites launched by the United States Department of Defense equally spaced in six orbit planes at about 20,000 km altitude. The satellite constellation, currently consisting of seven operating satellites, is expected to be complete by the early 1990s. Many types of scientific applications are uniquely suited to the precise positioning capabilities provided by GPS. The relatively high precision, low cost, mobility, and convenience of GPS receivers make GPS-based positioning attractive. Dense GPS ground networks are already operating in North

America, South America, Europe, and Japan to monitor cm-level crustal motions in geologically active regions. Initial results from GPS experiments since 1985 are encouraging and suggest that accuracies may be obtained equaling those available from other generally more restrictive techniques, such as Very Long Baseline Interferometry (VLBI) or satellite laser ranging (SLR). When the GPS constellation is complete, a worldwide ground tracking network equipped with advanced GPS receivers will enable sub-decimeter low-earth orbiter position accuracies to be achieved for satellites such as TOPEX/Poseidon [1] and the Earth Observing System (Eos) platforms [2, 3]. This worldwide tracking network will also be used to monitor earth orientation over timescales of less than one day [4], improve relative station positions at the cm level, determine absolute station positions relative to the geocenter with accuracy of better than 5 cm [5], enable global time transfer at the nanosecond level, and provide precise calibrations of path delays from the ionosphere and troposphere. The improved knowledge of earth orientation, station positions, time transfer, and media calibration will be used at NASA's Deep Space Network (DSN) tracking stations in support of navigation for planetary exploration missions. The GPS-based tracking network will also provide a meter-level orbit determination capability at the DSN for certain high-earth orbiters [6].

In this article, an overview of GPS signal structure and positioning techniques will be presented. A section describing the filter/smoother software developed and used at the Jet Propulsion Laboratory (JPL) for GPS orbit determination and parameter estimation will highlight some of the filtering techniques and algorithms which are especially useful in GPS-based least-squares parameter estimation. Recent high-accuracy GPS orbit and ground baseline results will also be presented to demonstrate the feasibility and potential of high-accuracy GPS-based navigation and positioning applications.

II. GPS Signal Structure and Positioning Techniques

The Global Positioning System is designed so that typically four to eight GPS satellites are visible simultaneously at any time from most locations in the world. The GPS satellites transmit down towards the Earth carrier signals at two L-band frequencies (1.227 and 1.575 GHz), which are modulated by a pseudorandom noise code, the P-code (Fig. 1). The two frequencies enable the user to remove most of the signal delay originating in the ionosphere. When four satellites are in view, the user equipped with a receiver which can receive the GPS P-code has enough information to solve for the user position and the user clock offset from GPS time. This is the simplest and most basic GPS positioning technique, often called *direct GPS tracking* (Fig. 2a). A second code, the coarse acquisition (C/A) code meant for acquiring and locking onto the GPS signal, can also be used for user positioning, but with somewhat degraded accuracy compared to the P-code. Part of the navigation message broadcast down on the P-code includes the ephemeris for each satellite and the clock offset of each satellite from the reference GPS time. The accuracy of the broadcast ephemeris (about 10–20 m) and the clock information currently limit user positioning accuracy to about 10–15 m with real-time techniques using the P-code. The P-code observable is often called a *pseudorange* since it measures the range to the satellite but includes offsets between the transmitter and receiver clocks.

To improve positioning accuracy through cancellation of clock errors and partial cancellation of ephemeris errors, *differential GPS tracking* techniques are employed (Fig. 2b). Instantaneous P-code positioning accuracy of 1–3 m is possible with differential GPS tracking. For certain military applications as well as for some real-time applications such as an earth orbiter docking with the space station, accuracies obtainable with instantaneous direct or differential GPS tracking are sufficient.

There are several strategies for reducing the GPS error budget further for high-accuracy applications, which include cm-level station determination, meter-level high-earth orbit estimation, cm-level earth orientation monitoring, and sub-nanosec time transfer. The high-precision strategies include use of precise GPS carrier phase tracking and averaging over several hours or more, use of dynamical information to reduce the number of degrees of freedom, and estimation of improved GPS orbits and clocks along with determination of other estimated parameters from the tracking data. The GPS carrier phase provides a very precise measure of *range change*, but is ambiguous in absolute range to an integer number of carrier wavelengths. Measurement noise with modern GPS receivers over five-minute intervals is typically several mm with the dual frequency combined carrier signal (to remove ionospheric effects). If the satellites are tracked for several hours, the signatures in the data enable estimation of the integer cycle ambiguities along with the other parameters. A more powerful approach is to process the P-code pseudorange, which can be one or two (or more) orders of magnitude noisier but provides a measure of absolute range, along with the carrier phase. This constrains the clocks and carrier phase range ambiguities so that the solutions are strengthened considerably.

Most commercial receivers provide pseudorange with measurement scatter of 60–200 cm over five-minute averaging intervals. Most of this scatter is due to multipath characteristics of the ground site and antenna. The Rogue receiver was designed at JPL with the goal of substantially reducing pseudorange measurement scatter. The Rogue, which features

digital baseband electronics, can track up to eight satellites simultaneously with dual-frequency carrier phase and pseudorange. A new antenna design shows considerable promise in reducing P-code multipath by an order of magnitude (Fig. 3). This design includes a drooped cross-dipole antenna with a non-absorbing backplane which has concentric choke rings machined from an aluminum disk spaced to maximally eliminate multipath signals. When GPS equipment such as the Rogue receiver and its new antenna design are routinely used in the field, a substantial improvement in tracking performance and system accuracy is expected.

III. Formulation of the Least-Squares Problem

As discussed above, to improve GPS-based tracking performance, GPS carrier phase and pseudorange can be received over a period of hours and parameters then estimated using dynamical model information. At JPL, the GPS orbit determination problem is reduced to a system of linear equations which can be solved with a batch-sequential process noise filter. This approach requires a moderately accurate nominal model for the GPS orbits and station locations so that only the linear terms in an expansion for deviations from this nominal model need be retained. It has been found that initial GPS epoch states should be accurate to about 1 km and receiver locations should be known to within a few hundred meters.[1] The initial GPS epoch states are numerically integrated with a multi-step Adams method[2] in the J2000 inertial reference frame [7]. Variational partial derivatives are computed relating the change in satellite position and velocity with respect to changes in the initial epoch states and with respect to force parameters. The Earth's gravity field is expressed in terms of a spherical harmonic expansion, and the gravitational effects of the sun, moon, and planets are represented as due to point masses. The JPL software includes the ROCK4 [8–10] GPS solar radiation pressure model, allows for estimation of arbitrary unmodeled accelerations on the satellite, and includes impulsive motor burns when needed to model GPS maneuvers. Typically the broadcast ephemeris or a more precise ephemeris produced by the Naval Surface Weapons Center (NSWC) is used for the nominal trajectory.

Precise earth models are used both to model the measurements and to compute the partials for measurements with respect to model parameters [11] as a function of time. The algorithms used are based on ones developed for Very Long Baseline Interferometry (VLBI), an extremely accurate astrometric technique which uses radio astronomical measurements of fixed point sources (quasars) [12] for deep space navigation and determination of ground baselines and earth orientation. The models include UT1-UTC, polar motion, nutation, precession, solid earth tides, ocean tidal loading, general relativistic clock corrections, and the Lanyi tropospheric delay mapping function [13], which relates the tropospheric delay at various elevations to its value at the zenith. Through the chain rule, the partials are referred to the GPS epoch states. The GIPSY (GPS Inferred Positioning SYstem) software is used for GPS data processing. The OASIS (Orbit Analysis and SImulation Software) software, developed at JPL[3,4] for covariance analysis and simulations, shares most programs with GIPSY but has a streamlined, simplified models module.

The difference, z, between each observation and its computed predicted value from the nominal model is calculated. The measurement equation is

$$z = \mathbf{A}_x\mathbf{x} + \mathbf{A}_p\mathbf{p} + \mathbf{A}_y\mathbf{y} + \nu \qquad (1)$$

where $\mathbf{A}$ is a row from the matrix of measurement partials, $\mathbf{x}$ is the satellite state vector (usually three position and three velocity components), $\mathbf{p}$ is the vector of process noise parameters, $\mathbf{y}$ is a vector of bias (constant) parameters, and ν is a zero mean white noise with $\langle\nu^2\rangle$ equal to the measurement noise variance. The OASIS/GIPSY filter is a multi-satellite program, so each satellite in turn has its associated state vector = $(\mathbf{x}^T,\mathbf{p}^T,\mathbf{y}^T)^T$, and these are ordered one after the other in the total state vector $\mathbf{X}$, with common parameters (such as station locations) placed at the end. The measurements are combined and an optimal least-squares solution for the estimated parameters determined in the filter. The filter divides the measurements into finite time intervals known as *batches*. Within each batch, all process noise parameters—parameters which are modeled as stochastically time-varying—are assumed to be piecewise constant. After the filter processes the measurements in a given batch, to update the estimates and covariance for the parameters a *time update* is performed to fold in the effects of process noise. Measurements are then processed in the next batch, and so on. After filtering is completed, a smoother works recursively backwards in time to update op-

[1] If the nominal model is not accurate enough, the output from the filter can be used as the new nominal model and the solution can be iterated.

[2] F. T. Krough, "Changing Stepsize in the Integration of Differential Equations Using Modified Differences," JPL Section 914 TM No. 312 (internal document), March 20, 1973.

[3] S. C. Wu, W. I. Bertiger, J. S. Border, S. M. Lichten, R. F. Sunseri, B. G. Williams, and J. T. Wu, *OASIS User's Guide, V. 1.0*, JPL D-3138 (internal document), April 1, 1986.

[4] S. C. Wu, W. I. Bertiger, J. S. Border, S. M. Lichten, R. F. Sunseri, B. G. Williams, P. J. Wolff, and J. T. Wu, *OASIS Mathematical Description, V. 1.0*, JPL D-3139 (internal document), April 1, 1986.

timally computed estimates and covariances when the presence of process noise requires it.

Both the OASIS and GIPSY software use the same filter for estimate/covariance computation. The filter offers the user the choice of two different mechanizations: the square-root information filter (SRIF), or the UD-factorized filter. Both mechanizations are based on the algorithms developed in [14] by Bierman. The smoother is formulated in terms of UD backwards pass recursions and works with output from either the SRIF or UD filter. Both the filter and the smoother make heavy use of the Bierman Estimation Subroutine Library (ESL) [15].

A. UD Filter Formulation for Measurement Processing

The conventional Kalman filter has a measurement update mechanization based on the *covariance matrix*, **P**. Let the estimate vector and covariance matrix be **X** and **P**, with the convention that ~ denotes quantities before measurement updating and ^ denotes quantities after the measurement update. Then

$$\begin{aligned}\hat{\mathbf{X}} &= \tilde{\mathbf{X}} + \hat{\mathbf{K}}(z - \mathbf{A}\tilde{\mathbf{X}}) \\ &= \tilde{\mathbf{X}} + (\hat{\mathbf{G}}/\alpha)(z - \mathbf{A}\tilde{\mathbf{X}}) \\ \hat{\mathbf{P}} &= \tilde{\mathbf{P}} - (1/\alpha)\hat{\mathbf{G}}\hat{\mathbf{G}}^{\mathrm{T}}\end{aligned} \tag{2}$$

where **A** is a row vector of measurement partials, **G** is the *normalized* Kalman gain vector, which is related to the unnormalized Kalman filter gain, **K**, by

$$\hat{\mathbf{G}} = \tilde{\mathbf{P}}\mathbf{A}^{\mathrm{T}} = \alpha\hat{\mathbf{K}} \tag{3}$$

and $\alpha = \mathbf{A}\tilde{\mathbf{P}}\mathbf{A}^{\mathrm{T}} + r$ is the innovations, or prediction residual variance. The measurement variance is r. It is assumed here that the vector of observation errors, v_i, is described by $E(v_i) = 0, E(vv^T) = \mathbf{P}_v$, for $i = 1, \ldots, m$, and $\mathbf{P}_v = \mathrm{Diag}(r1, \ldots, r_m)$ for the measurement variances. In the case of correlated measurement noise, whitening procedures can be used to uncouple the measurements and yield diagonal $\mathbf{P}_v$ [14], so the formulas presented here are valid without loss of generality.

The conventional Kalman measurement update (Eq. 2) has been shown to be sensitive to computer roundoff with sometimes catastrophic loss of accuracy from imperfect cancellation when positive quantities are differenced. Conventional Kalman algorithms have also exhibited sensitivity to numerical ill-conditioning [14, 16]. A comprehensive comparison of conventional, stabilized, and factorized formulations of the Kalman filter for a spacecraft navigation problem [16] demonstrated convincingly the superior numerical characteristics of the factorized Kalman filter approach. Ill-conditioning with unfactorized Kalman filters is sometimes attributed to large a priori state uncertainties and relatively small data covariances. These very attributes, however, typify many GPS earth orbiter problems relying on the GPS carrier phase data type: the carrier phase data variance is on the order of 10^{-5} m^2 while the a priori position covariance could be between 1 and 10^6 m^2. Another filter characteristic associated with ill-conditioning is a very low level of process noise. However, low process noise levels are common in high-precision GPS applications when stochastic models are used to model slowly varying tropospheric delay variations, GPS force parameters, and stable hydrogen maser station clocks. Near-singular covariance matrices are sometimes encountered in GPS orbit filtering because of different receiver characteristics. At some sites, GPS receivers were operated side by side in experiments which took place in 1985 where one receiver was capable of producing GPS carrier phase and P-code pseudorange and the other could only produce carrier phase data (codeless). The clock offset for the code receiver could be determined much more precisely than for the phase-only receiver: the clock variances were typically 2.5×10^{-7} μsec^2 for the code receivers while codeless receiver clock variances are typically 10^4 μsec^2. Furthermore, since these clock parameters are often modeled with process noise, their variances vary considerably in the course of a run as satellites move through different geometries with good and bad observability. With GPS scenarios, severe numerical difficulties were sometimes encountered when mapping orbits and baselines to various coordinate systems when using the unfactored covariance matrix; with factored or square-root form, however, these mappings were stabilized and no numerical problems have been noted. Experience at JPL with deep space tracking estimation software has also resulted in complete conversion to factorized (or square-root) Kalman filter mechanizations in the orbit determination program used for missions involving such spacecraft as the Voyager, Magellan, and Galileo interplanetary probes. With efficient algorithms [14-16], there is only an insignificant penalty in computation speed when using factorized instead of conventional Kalman filters.

An extremely stable factorized version of the Kalman measurement update equations exists for the **U** and **D** factors of the covariance matrix, where **U** is an upper triangular matrix and **D** is a diagonal matrix:

$$\mathbf{P} = \mathbf{U}\mathbf{D}\mathbf{U}^{\mathrm{T}} \tag{4}$$

The method used is an upper triangular UD Cholesky square-root-free factorization with the geometric form reduction described in [14]. In order to save storage, **U** is vector stored, and the factorization is chosen so that **U** has unity on its diagonals and **D** can be stored in those locations. It is con-

venient to store the estimates, $\mathbf{X}$, in the last column appended on the end of the UD matrix.

With the UD factorization, the measurement update can be expressed as

$$\hat{\mathbf{P}} = \hat{\mathbf{U}}\hat{\mathbf{D}}\hat{\mathbf{U}}^{\mathrm{T}} = \tilde{\mathbf{U}}(\tilde{\mathbf{D}} - c\mathbf{V}\mathbf{V}^{\mathrm{T}})\tilde{\mathbf{U}}^{\mathrm{T}} \tag{5}$$

where

$$\mathbf{V} = \tilde{\mathbf{D}}\mathbf{F}$$

$$\mathbf{F} = (\mathbf{A}\tilde{\mathbf{U}})^{\mathrm{T}}$$

The scalar $c = 1/\alpha = 1/(r + \mathbf{V}^{\mathrm{T}}\mathbf{F})$ is computed from the prior covariance and the current measurement noise. Thus, the normalized Kalman gain can be expressed in terms of the UD factors as

$$\hat{\mathbf{G}} = \tilde{\mathbf{U}}\tilde{\mathbf{D}}\tilde{\mathbf{U}}^{\mathrm{T}}\mathbf{A}^{\mathrm{T}} = \tilde{\mathbf{U}}\mathbf{V} \tag{6}$$

The measurement update algorithm used in the OASIS/GIPSY filter is the Bierman-Carlson-Gentleman update [14, 16, 17]. This algorithm avoids explicit differencing when computing updated diagonals because explicit differencing for these terms makes the update prone to loss of accuracy due to imperfect cancellation, leading to negative diagonals in extreme cases.

The UD filter processes measurements one at a time. Before updating, each measurement is tested for consistency with the prior estimates and covariance. If the measurement fails the test, it is considered to be an outlier and not processed. The prediction residual must satisfy the criterion

$$(z - \mathbf{A}\tilde{\mathbf{X}})^2 \leqslant TST\alpha \tag{7}$$

where TST is the level of acceptance and α is the innovations variance defined above. For example, $TST = 9$ is a 3-σ test. If Eq. 7 is satisfied, the estimates and covariance are updated.

B. SRIF Formulation for Measurement Processing

The SRIF data equations are

$$\tilde{z} = \tilde{\mathbf{R}}\tilde{\mathbf{X}} + \tilde{v} \tag{8}$$

where

$$\tilde{\mathbf{P}} = \tilde{\mathbf{R}}^{-1}\tilde{\mathbf{R}}^{-\mathrm{T}}$$

and estimates are retrieved as

$$\mathbf{X} = \mathbf{R}^{-1}z$$

The square-root information array $[\mathbf{R}:z]$ is analogous to the UD-factored covariance with estimates in the last column of the UD matrix. The square-root information matrix, $\mathbf{R}$, like the $\mathbf{U}$ matrix, is upper triangular and vector stored. Note that for the SRIF, the noise v is zero mean as before but has unit covariance, so z and v have been normalized by the measurement noise.[5] The SRIF data processing algorithm in the OASIS/GIPSY software follows [14] and [18] in applying orthogonal Householder transformations, $\mathrm{T_H}$, to an augmented information array

$$\mathrm{T_H}\begin{bmatrix}\tilde{\mathbf{R}} & \tilde{z}\\ \mathbf{A} & z\end{bmatrix} = \begin{bmatrix}\hat{\mathbf{R}} & \hat{z}\\ \mathbf{0} & e\end{bmatrix} \tag{9}$$

The measurement partials (normalized) are in $\mathbf{A}$, and e contains information about the post-fit residuals. The matrix $\mathbf{A}$ ordinarily holds a subset of the data, since on some computers, available memory or disk space limits how many measurements can be processed at once. When process noise is included, the measurements to be processed together in a buffer must lie in the same time batch. The ith row in $\mathbf{A}$ contains the ith measurement in this measurement buffer, so when the ith elementary Householder transformation is applied, only the ith row of $\mathbf{R}$ and all columns to the right of column i in $\mathbf{A}$ are affected. The Householder transformation, as implemented in the filter, maintains the upper triangularity of the $\mathbf{R}$ matrix [14, 18].

The effect of the size of the measurement buffer on the speed of the SRIF on a DEC Microvax II is shown in Fig. 4. Beyond a buffer of about 50 measurements, little increase in speed is seen. However, for very small buffer sizes, the Householder transformation becomes inefficient. The reason for this is that, based on the operation counts in [14], for additions and multiplications the ratio of (overhead)/(total processing time) in processing each measurement buffer with M_b measurements is $3/(3+2M_b)$ and $1/(1+2M_b)$, respectively.

There is also an additional amount of overhead from the N square roots, N divisions, $2N$ additions, and N multiplications needed for each buffer being processed, where N is the number of parameters estimated. The penalty from these extra operations depends somewhat on the relative CPU speed of these

[5] To distinguish these normalized quantities from the unnormalized ones from the discussion of the UD filter, we represent them without italics.

operations. The case shown in Fig. 4 corresponds to 3666 measurements with 192 estimated parameters for a SRIF running on a DEC Microvax, where square roots and divisions are about 8 and 1.5 times as expensive as additions or multiplications, respectively. The composite ratio of overhead to processing time was calculated and would be 60 percent for this run with $M_b = 1$, and less than 1 percent for $M_b = 100$, in rough agreement with the curve in Fig. 4.

C. Process Noise

Stochastic processes in the GPS orbit software are assumed to be piecewise constant over a specified batch interval. Currently, first-order Gauss-Markov random processes models are used. At the end of a batch, a process noise time update adds noise to the covariance matrix and thus causes the time-varying behavior of the stochastic parameters. The process noise time update for the jth batch maps the estimates and covariance for the stochastic parameters into the batch $j+1$:

$$\begin{aligned} \mathbf{x}_{j+1} &= \mathbf{x}_j + \Phi_p(j)\mathbf{p}_j \\ \mathbf{p}_{j+1} &= \mathbf{M}_j\mathbf{p}_j + \mathbf{w}_j \\ \mathbf{P}_{j+1} &= \Phi\mathbf{P}_j\Phi^{\mathrm{T}} + \mathbf{Q} \end{aligned} \tag{10}$$

where

$$\Phi = \begin{bmatrix} \mathbf{I}_x & \Phi_p(j) & 0 \\ 0 & \mathbf{M}_j & 0 \\ 0 & 0 & \mathbf{I}_y \end{bmatrix}$$

and, as in Eq. (1), the estimated parameters are partitioned into satellite states, process noise parameters, and bias (constant) parameters

$$\mathbf{X} = \begin{bmatrix} \mathbf{x} \\ \mathbf{p} \\ \mathbf{y} \end{bmatrix} \tag{11}$$

$\mathbf{M}$ is a diagonal process noise mapping matrix. The process noise $\mathbf{w}_j$ is a random process with zero mean and for the ith process noise parameter,

$$E(w_{ij}w_{ik}) = q_{ij}\delta_{jk} \tag{12}$$

with the covariance matrix $\mathbf{Q}$ zero except for diagonal elements q_i in the jth batch, and δ_{jk} is the Kronecker delta function. The diagonal entries of $\mathbf{M}$ are given by

$$m_{ij} = \exp\left[-(t_{j+1} - t_j)/\tau_{ij}\right] \tag{13}$$

where t_j is the start time for the jth batch and τ_{ij} is the time constant for the ith stochastic parameter at the jth batch. The corresponding diagonal entry in the matrix $\mathbf{Q}$ is

$$q_{ij} = (1 - m_{ij}^2)\sigma_{iss}^2 \tag{14}$$

where σ_{iss}, the steady-state sigma for the ith stochastic parameter, is the noise level which would be reached if the system were left undisturbed for a time much greater than τ.[6] For white process noise, $\tau = 0$, $m = 0$, and as can be seen in Eq. (10), the filter resets the covariance for the process noise parameters at the end of each batch, including zeroing of off-diagonal terms and putting in q for the variance on the diagonal. The opposite limiting case is the random walk: here both σ_{ss} and τ are unbounded ($\tau = \infty$) and a steady-state is never reached. For the random walk, $\mathbf{M}$ is equal to the identity matrix, and it is the rate of change of the process noise covariance, $\dot{q} = dq/dt = \Delta q/\Delta t$, which characterizes the process, where Δt is the batch size and Δq is the amount of noise added per batch. The Allan variance [19], $\sigma_A^2(\Delta t)$, which is often used to characterize clock and atmospheric fluctuations [12], can be defined in terms of $\dot{q}$:

$$\sigma_A^2(\Delta t) = \dot{q}/\Delta t \text{ (random walk)} \tag{15}$$

Thus a random walk process has a slope of -1 for the log-log relation between the Allan variance and Δt.

The matrix $\Phi_p(j)$, represents the *deterministic* portion of the time update and is nonzero only when there is a dynamic coupling between process noise parameters and satellite states. $\mathbf{M}$ contains the *stochastic* portion of the time update. $\mathbf{x}_j$ represents the *pseudo-epoch state* of the spacecraft [14]. The *current state*, $\mathbf{x}(t)$, would be mapped according to

$$\begin{bmatrix} \mathbf{x}(t) \\ \mathbf{p}(t) \\ \mathbf{y} \end{bmatrix}_{j+1} = \begin{bmatrix} \Phi_x(t_{j+1}, t_j) & \Phi_p(t_{j+1}, t_j) & \Phi_y(t_{j+1}, t_j) \\ 0 & \mathbf{M}_j & 0 \\ 0 & 0 & \mathbf{I}_y \end{bmatrix} \begin{bmatrix} \mathbf{x}(t) \\ \mathbf{p}(t) \\ \mathbf{y} \end{bmatrix}_j + \begin{bmatrix} 0 \\ \mathbf{w} \\ 0 \end{bmatrix}_j \tag{16}$$

The *pseudo-epoch state*, $\mathbf{x}_j$, is defined relative to the current state, $\mathbf{x}(t)$, from

[6] Although σ_{ss} and τ can vary with time, the subscript j has been left off σ_{ss} for simplicity of notation.

$$x(t_j) = \Phi_x(t_j, t_0)x_j + \Phi_y(t_j, t_0)y$$

$$x_j = \Phi_x^{-1}(t_j, t_0)\,[x(t_j) - \Phi_y(t_j, t_0)y] \tag{17}$$

With this definition, if the pseudo-epoch state is used in the filter instead of the current state, the time update of Eq. (10) results:

$$\begin{bmatrix} x \\ p \\ y \end{bmatrix}_{j+1} = \begin{bmatrix} I_x & \Phi_p(j) & 0 \\ 0 & M_j & 0 \\ 0 & 0 & I_y \end{bmatrix} \begin{bmatrix} x \\ p \\ y \end{bmatrix}_j + \begin{bmatrix} 0 \\ w \\ 0 \end{bmatrix}_j \tag{18}$$

The mapping matrix $\Phi_p(j)$ used in the pseudo-epoch state filter is calculated from the variational partials:

$$\Phi_p(j) = [\Phi_x(t_{j+1}, t_0)]^{-1}\,\Phi_p(t_{j+1}, t_0)$$

$$-[\Phi_x(t_j, t_0)]^{-1}\,\Phi_p(t_j, t_0) = \left.\frac{\partial x_{j+1}}{\partial p_j}\right|_{p_j = 0} \tag{19}$$

The use of the pseudo-epoch state formulation saves considerable computation in the filter and smoother since the UD time update is accomplished with sparse matrix multiply routines. When no dynamic stochastic parameters are present, the pseudo-epoch state is the same as the true epoch state. Because of the pseudo-epoch state formulation, most of the mapping matrix is filled with zeros or ones (see Eq. 18). The state vector **X** is arranged so that the satellite state for each satellite and the associated stochastic parameters are grouped at the top. A subroutine loop performs the sparse matrix multiply to update the **U** matrix and estimates for each spacecraft in turn, making efficient use of knowledge of the implicit zeros and ones for the deterministic mapping. After the deterministic Φ_p mappings for all the satellite are finished, the stochastic **M** mappings are performed to update the process noise states. The UD stochastic update is accomplished with the Bierman-Thornton one-at-a-time update [14, 17, 20]. The deterministic portion of the SRIF time update also takes advantage of the sparse mapping matrix structure. The stochastic SRIF time update uses Givens transformations which exploit the upper triangular structure of the **R** matrix.

Both the UD and SRIF time updates use subroutines of the ESL for most of the matrix operations. The SRIF stochastic update includes calculation of the smooth gain arrays which must be saved if smoothing will be done later. For the UD filter, these smooth gains are calculated in a separate routine which can be skipped if smoothing will not be needed.

D. Smoothing

The OASIS/GIPSY smoother incorporates Bierman's modification of the Rauch-Tung-Streibel (RTS) smoother [21], known as the BRTS, including the new reformulation of Bierman's original UD smoother [22, 23]. The smoother algorithm makes use of a decomposition of the linear model dynamical equations so that rank-1 and rank-2 matrix modifications can be substituted for more complex (and costly) covariance updates. The smoothing algorithm uses the UD formulation, is based on numerically stable Givens reflections, and runs "backwards" in time using a recursive method for generating smoothed estimates and smoothed UD factors. The last (terminal) filter UD or SRIF matrix is used to initialize the smoother, so in the case of the SRIF, the terminal square-root information array is inverted to UD form. The smoother has considerable flexibility in the handling of singular and near-singular covariance matrices. As with the deterministic and stochastic filter time updates, the OASIS/GIPSY implementation of Bierman's smoothing algorithm takes advantage of the sparse matrix structure which typifies GPS scenarios and orders parameters to minimize CPU cycles, memory requirements, and disk storage.

E. Evaluation of Filter Mismodeling

The OASIS/GIPSY filter has a number of options for evaluating filter models used for parameter estimation and covariance analysis. These include *consider analysis* for both the UD and SRIF formulations, and a unique *evaluation mode* available only with the UD filter.

Consider parameters are usually bias parameters not included in the estimated parameter state vector. From the measurement partials, the sensitivity of estimated parameters to these considered (not estimated) parameters can be computed in the filter. There are several reasons for not estimating a parameter: (1) certain parameters, such as fiducial station locations, may be held fixed in order to define a reference frame and/or length scale; (2) it may be computationally impossible to adjust certain parameters, such as all the coefficients in a gravity field; (3) a physical effect cannot be modeled adequately to produce a reliable estimate, yet it is still desirable to calculate the penalty for leaving it out of the filter model (state vector). By including the effects of considered parameters, the ordinarily overly optimistic computed covariance for the estimated parameters is degraded somewhat depending on the sensitivities, and a more realistic covariance may result.

Let y_c be the unestimated considered parameters with measurement partials A_c. Then the sensitivity is [14]

$$S = \frac{\partial(X - \hat{X})}{\partial y_c} = -\hat{P}A^T P_v^{-1} A_c \tag{20}$$

where the $\sim$ denotes the quantities computed from the filter measurement and time updates without including the effects of the y_c parameters, and P_ν is the measurement noise covariance matrix. The *consider covariance*, which includes effects from both estimated and considered parameters, is defined as

$$P_{con} = \hat{P} + SP_cS^T \tag{21}$$

where P_c is the covariance matrix for the considered (unadjusted) parameters.

Both the SRIF and UD filter implementations in the GIPSY/OASIS software can handle any parameter as estimated or considered. However, only the UD filter has more general filter error evaluation capabilities, of which consider analysis is one type. The general error evaluation algorithm [24] permits evaluation of the effects of designing a filter without the correct data noise, a priori covariance, data weights, or process noise model. A *truth model* and filter model are specified, and the evaluation mode of the UD filter allows the user to assess the effects of mismodeling on filter accuracy. Under real conditions, the truth model is not actually known, so a filter analyst usually tries to look at a range of possible truth models to see if, over a range of reasonable truth models, the filter results are especially sensitive to any parts of the filtering strategy being used. The goal is to design a filter model which is reasonably accurate based on available information about the problem, but which is also stable so that the results will not be strongly degraded if slightly incorrect filtering parameters are used. In [25] is an example of a comprehensive filter evaluation which studied the use of stochastic solar radiation pressure models for GPS orbit determination. A number of process noise inputs were identified for which the filter showed little sensitivity to mismodeling. These process noise models were later used successfully for estimation of small GPS accelerations over arcs of several weeks (also see Section IV of this article).

In the evaluation mode, the filter uses suboptimal Kalman gains saved in an evaluation file from an earlier filter which is run purposely with what is believed to be an incorrect model in order to generate suboptimal gains. The measurement update is expressed as

$$\hat{P} = (I - \hat{K}A)\tilde{P} + \alpha(K - \hat{K})(K - \hat{K})^T \tag{22}$$

where the *optimal* Kalman gain is $\hat{K}$ and the arbitrary gain from the evaluation file is K. Let $\bar{P} = (I - \hat{K}A)\tilde{P}$ and $\bar{U}\bar{D}\bar{U}^T = \bar{P}$. Then $\hat{K}$ and α are computed using the measurement update formulas in Eqs. (2–4), and the vector $\lambda = K - \hat{K}$ is formed. A rank-1 update computes the UD covariance factors:

$$\hat{U}\hat{D}\hat{U}^T = \bar{U}\bar{D}\bar{U}^T + \alpha\lambda\lambda^T \tag{23}$$

The time update in the evaluation mode follows the same form as the original filter time update except that the original filter stochastic time constants and process noise sigmas are replaced with the evaluation mode time constants and process noise sigmas.

F. Performance Comparisons Between the UD Filter and the SRIF

The dual-filter option in the OASIS/GIPSY software facilitates comparisons between the UD and SRIF programs. Many tests have been conducted to examine the numerical stability and speed of these two filters. At this time, they appear to be equally stable and numerically sound. However, there can be a substantial difference in processing speed, depending on the type of problem being filtered. Our experience with timing the UD and SRIF algorithms matches very closely the predictions in [14]. The SRIF measurement processor is about 33 percent faster than the UD measurement processor. For time updates, however, the UD algorithm is substantially faster when smoothing gains are not needed. If smoothing gains are computed in the filter for later use in smoothing, then once again the SRIF runs faster. Smoothing itself takes essentially the same amount of time whether the UD or SRIF filter was run first. For any specific filter run, the comparison between SRIF and UD run times depends on the number of stochastic parameters, the number of batch intervals, and the number of measurements. For typical GPS orbit estimation scenarios involving the geodetic and low-earth orbiter applications described below, the SRIF is as much as 50 percent faster than the UD filter for complicated cases requiring smoothing. If the sensitivities in a consider analysis are needed for stochastically estimated parameters, the sensitivity matrix must also be smoothed. Sensitivity smoothing in the OASIS/GIPSY filter occurs in a natural and efficient way with the SRIF, while the UD sensitivity smoothing is usually substantially slower. The UD filter is about 25 percent faster than the SRIF in simple runs when no smoothing is needed.

With the UD formulation in OASIS/GIPSY, the analyst is permitted to have the variance of a parameter equal zero. In certain analyses, such as a case where it is desired to constrain a parameter to a specific value, this capability can be useful. On the other hand, the SRIF formulation permits zeros on the diagonals of the information array, corresponding to an infinitely large covariance. As discussed above, the SRIF tends to be faster in situations when many measurements are being processed or when smoothing is needed. Only the UD filter, however, has an *evaluation mode* for studying filter mismodeling. The decision to fully implement both filter mechanizations in the OASIS/GIPSY software allows the analyst full

flexibility in the selection of the most efficient and appropriate filter for each specific situation.

IV. GPS Positioning Applications

Even though only seven GPS satellites are currently operating, high-accuracy geodetic results have already been obtained. In addition to the geodetic studies carried out with the existing limited set of satellites, numerous covariance analyses and simulations have been conducted in preparation for the full 21-satellite constellation expected to be operational in the early 1990s. A number of new approaches to high-accuracy earth-orbiter and ground positioning applications show great promise for demanding projects of the future such as TOPEX and Eos. In this section, a sampling of these results and new tracking techniques will be presented, with emphasis on how the orbit determination and filtering strategy play a role in GPS-based positioning and navigation.

A. Ground Station Positioning Results

A number of GPS campaigns and experiments took place in 1984 and 1985 [26, 27], in which typically 5–10 GPS receivers were located at sites of geodetic or geophysical interest. Baseline results showing precision and accuracy of 2–4 parts in 10^7 relative to baseline length were initially reported [27–29], with quality of the baselines generally assessed by comparison to VLBI and SLR, and by daily repeatability of the solutions. To reach these accuracies, GPS orbits were improved through estimation, generally with single-batch least-squares fits with doubly differenced dual-frequency carrier phase. Double differencing is a technique for cancellation of GPS and station clock errors which requires simultaneous mutual visibility. In most, but not all of these cases, fiducial or reference ground sites were held fixed where GPS receivers were collocated with very precisely determined VLBI antennas in order to establish a reference frame and length scale. Without orbit improvement, GPS positioning results obtained using broadcast ephemerides only were, in most cases, about an order of magnitude worse.

In [30], results were presented from one of the 1985 GPS experiments showing accuracy and daily repeatability of 1–2 parts in 10^7 for baselines up to 313 km. This improvement was due to a number of factors, including combining more than one eight-hour daily pass for orbit estimation, bias fixing, and an improved fiducial network geometry. Bias fixing is a technique for applying the constraint that the carrier phase range ambiguity be an integer number of wavelengths. This ambiguity is determined for as many baseline–satellite combinations as possible, and the overall solutions are readjusted while the ambiguities are fixed at their integer values [31, 32]. One approach to bias fixing [33] uses the SRIF formulation to optimally adjust all the biases and other estimated parameters and to update the covariance matrix with an algorithm which is fast and does not require iterating or expensive refiltering. The major weakness with solutions from only carrier phase data is a relatively low accuracy in the eastern baseline components due to the predominantly north-south GPS satellite tracks. Bias fixing can largely remove this weakness in the eastern directions.

Kalman (factored covariance) filter-oriented approaches to the GPS estimation problem with emphasis on orbit determination further improved baseline results to the level of 2–4 parts in 10^8 [34] for baseline distances of more than 1000 km. The key strategies emphasized included multi-day (one-week) Kalman filtered orbit solutions, simultaneous parameter estimation, determination of three (instead of the usual two) GPS solar radiation pressure parameters, random-walk models for zenith troposphere delay fluctuations, and simultaneous processing of carrier phase and pseudorange data. The pseudorange data tightly constrain the clocks and carrier phase ambiguities, improving the results particularly in the east for baselines and down-track for orbits. The transmitter and receiver clocks are estimated as white noise parameters, leading to essentially the same results as double differencing but with considerably less complexity. Direct comparisons between independent GPS orbit solutions [34] indicated orbit precisions of 1–2 m had been achieved. Further refinements to the filtering strategies have produced improved GPS accuracies of better than 1 m for orbits and 1–2 parts in 10^8 for baselines up to 2000 km [35]. These additional refinements included modeling of a GPS maneuver which enabled the data arcs to be extended from one to two weeks and constrained stochastic GPS force parameter estimation. Figure 5 shows locations of ground receivers from North American GPS experiments in 1985 and 1986. Figure 6 shows the improvement in daily baseline repeatability using two-week orbit arcs when process noise models for force parameters were used. For arcs of one week or less, it was not necessary to use stochastic force models. In these experiments, all the measurements were confined to the same eight-hour interval each day and it was not possible to determine whether stochastic solar pressure or stochastic three-dimensional thrust parameters fit the data better. It is expected that in the future, with longer arcs and a more global tracking network, the physical nature of these stochastic forces will be better understood.

Orbit verification to better than 1 m is illustrated in Figs. 7 and 8. In each test, the data were partitioned into one-week arcs and independent orbit solutions were obtained and compared. The interleaved arc orbit comparison (Figs. 7a and 7b) shows sub-meter repeatability for two well-tracked satellites. A more strenuous test using orbit prediction is shown in Figs. 8(a) and 8(b), demonstrating sub-meter agreement for

GPS 8. Figure 8(b) also shows how the results improve when pseudorange is processed with carrier phase and stochastic models for tropospheric delay fluctuations are used.

A convincing test of GPS-based positioning accuracy comes from comparisons between 2000-km GPS-determined baselines with VLBI measurements of the same baselines. VLBI is a completely independent geodetic system referenced to the inertial quasar-defined frame, whereas the GPS-based techniques use fiducial points tied to the VLBI system through local surveys to determine accurate GPS orbits, thereby transferring fiducial control to other stations whose coordinates are estimated. Figure 9 shows that 2000-km baselines determined with GPS agree with VLBI to better than 1.5 parts in 10^8 accuracy, which is close to the advertised accuracy of the VLBI system itself.

Recent improvements in bias fixing techniques [33, 36, 37] have enabled successful ambiguity resolution over regions up to 2000 km in extent. In these cases, cm-level agreement between GPS and VLBI has been achieved in horizontal baseline components with single-day arcs, provided that the stations are spaced appropriately in these regions so that ambiguity resolution can proceed over all or nearly all station–satellite combinations. To reach high accuracy in the vertical baseline components as well, multi-day arcs seem to be needed at the present time, but with worldwide tracking networks and additional GPS satellites, shorter tracking arcs will be adequate. GPS solutions seem to show lower scatter than VLBI solutions in the vertical component, perhaps because the GPS measurements are robust enough to estimate the troposphere stochastically with sub-centimeter precision.

B. Earth Orbiter Positioning with GPS

The TOPEX/Poseidon satellite [38], scheduled for launch in late 1991, will lead to significant progress in the study of the interaction of the oceans and climate on a global scale. To understand global weather patterns, experiments like TOPEX are needed to study the world ocean's circulation. The oceans redistribute heat, with warm currents carrying one-half of the excess heat from the tropics to the poles. The seas hold much more heat than the atmosphere and moderate the seasonal temperature fluctuations. Global circulation is observable from space because ocean movement causes bulges and depressions. The sea surface height can be measured with satellite altimeters, as Seasat demonstrated in 1978. The detailed sea surface topography is a complicated function of ocean currents and the geopotential. A complete analysis of TOPEX data will separate the mean sea surface, or marine geoid, from time-varying currents, using repeat orbits and averaging techniques. The ability to map global ocean currents with TOPEX will have far-ranging benefits affecting weather and climate prediction, fishing, commerce, and shipping. The El Niño effect, which is a huge atmospheric seesaw leading to weather reversals, floods, economic hardship, heavy rain, and droughts, may be predictable in advance and eventually better understood through monitoring of the ocean surface with satellites like TOPEX, since it is typically accompanied by a raised mean ocean level of about 20 cm and an increase in the ocean temperature of about 2 deg C off the western coast of South America.

TOPEX will fly in low-earth orbit at about a 1334-km altitude, carry an altimeter precise to about 2 cm to determine the range between the satellite and the sea surface, and will map the topography of the ocean surface. A key to the success of the mission is that the TOPEX orbit altitude error be kept below about 13 cm during the mission. Several different orbit determination techniques will be used on TOPEX, including ground-based laser ranging, but TOPEX will also carry a GPS flight receiver as part of an experiment to demonstrate precise low-earth satellite orbit determination. The TOPEX GPS demo is the first of the anticipated high-precision earth orbiter GPS applications for satellites at a wide range of altitudes, including geosynchronous as well as highly elliptical orbits.

The major error source for differential GPS dynamic tracking of TOPEX [1] is uncertainty in the model for the geopotential. This is also expected to be the limiting error for other tracking techniques [38]. Recent attention has focused on an orbit determination approach using differential GPS in which the orbit filter is designed to desensitize the results as much as possible from gravity errors [39]. A three-dimensional fictitious force is modeled as process noise and estimated in this approach, referred to as *reduced dynamic tracking*. The role these stochastic force parameters play in the orbit filter is controlled through the process noise τ and σ_{ss} (Eqs. 11–14), and depends on the accuracy of the dynamic models for the satellite. If the dynamic models are very poor, the proper strategy is to set $\tau \to 0$ and $\sigma_{ss} \to \infty$, and this is the limiting case of *non-dynamic tracking*. The other limiting case is *purely dynamic tracking* in which maximal weight is given to the dynamic models and the stochastic force parameters are essentially turned off ($\tau \to \infty$ and $\sigma_{ss} = 0$). In between is *reduced dynamic tracking*, where a finite τ and σ_{ss} determine how much reliance is placed on the dynamics and to what extent the unmodeled forces will be fitted out with the data. Although gravity is the major error source for TOPEX, the techniques used to minimize gravity-related orbit errors on TOPEX will also be useful for minimizing virtually any mismodeled force for other satellites using differential GPS tracking.

Figure 10 compares predicted performance of non-dynamic, reduced-dynamic, and dynamic techniques for TOPEX orbit

determination with GPS. Six globally distributed GPS ground receivers and the one TOPEX flight receiver were assumed to produce 5-cm pseudorange and 0.5-cm carrier phase over five-minute data intervals in a single two-hour arc for this covariance study. This level of performance can be achieved only with advanced receiver and antenna design, but current results with the Rogue receiver/antenna are very encouraging and indicate that these accuracies can be met (Fig. 3). The predicted altitude error shown in Fig. 10 for the dynamic solution strategy is dominated by the gravity field error, assumed to be 50 percent of the difference between the GEML2 and GEM10 fields. A comparison with the covariance matrix for the GEM-T1 [40] gravity field shows that representing the gravity error with the 50-percent geopotential difference for this analysis produces about the same results as produced with the current (GEM-T1) gravity field covariance. The large (~25-cm) excursions for the dynamic tracking approach occur over regions of the earth where the gravity field is poorly known, such as over the oceans. However, these oceanic regions are the key regions for an oceanographic experiment such as TOPEX. The non-dynamic approach also suffers from occasional sudden increases in the altitude error, primarily due to times of weaker viewing geometry. Since the non-dynamic tracking solutions are more data-intensive, they are more sensitive to times when viewing geometry is compromised. The reduced dynamic strategy performs best overall. The stochastic force parameter estimation (τ, σ_{ss}) was chosen to be optimal for a gravity field accurate to about the level of the current GEM-T1 field, but as pointed out in [39], even if the accuracy of the gravity field is only approximately known, the results are insensitive to the stochastic model as long as a relatively conservative approach is taken. This is one of the main advantages of the reduced dynamic tracking strategy.

The reduced and non-dynamic techniques compensate not only for gravity mismodeling, but also for *any* type of force or acceleration affecting spacecraft motion, such as drag, radiation pressure, gas leaks, maneuvers, etc. Estimation of fictitious thrust parameters for the GPS orbits themselves when tracking over relatively long (two-week) arcs (Fig. 6) is a simple example of the application of reduced dynamic concepts to satellites in high-earth orbits. It was found that the results in Fig. 6 showed very little sensitivity to τ and σ_{ss} over a wide range of values, as predicted in [39]. The GPS orbit strategy, however, still places very high weight on dynamic models since the constrained stochastic forces being estimated represent a tiny perturbation to the purely dynamic orbit determination.

C. Other Related GPS Applications

Certain GPS applications show great promise but require a global tracking network and a full GPS constellation, such as earth orientation monitoring [4]. Ultimately, the filtering and estimation strategy may be a major factor in the utility of GPS for earth orientation because one of the advantages of GPS is the high time resolution it provides. Another example of the importance of Kalman filtering is the determination of tropospheric zenith delay parameters as part of the GPS orbit determination process. GPS-based techniques have the potential of tracking tropospheric fluctuations at sub-centimeter levels with resolution of a few minutes. A GPS-based network for earth orientation monitoring, troposphere calibration, and determination of geocentric station coordinates is being studied for use in the Deep Space Network since these are major limiting errors for deep space navigation and planetary exploration. GPS tracking will be able to determine the location of the geocenter relative to any set of ground stations with an accuracy of better than 5 cm [5], in addition to its cm-level *relative* station positioning capability. The NSWC precise ephemeris, which is determined from a worldwide Air Force tracking network and is more accurate than the 10–20-m ephemeris broadcast down on the P-code, is currently determined along with values for earth orientation parameters [41] using a SRIF and RTS smoother [42] and process noise models for polynomial clock coefficients, troposphere parameters, and solar pressure coefficients. GPS also has the potential for global time transfer at the sub-nanosec level, which would hold great benefits for the Deep Space Network and other radio astronomy observatories.

If GPS antennas are placed at different points on an airplane, the attitude of the aircraft can in principle be determined from GPS measurements. An experiment was recently conducted [43] to demonstrate aircraft position, velocity, and attitude determination using GPS for a synthetic aperture radar experiment to study ocean currents, and the data are being analyzed at JPL. GPS receivers can also be placed on ships and buoys for research in seafloor geodesy [44], a relatively new field.

There are numerous real or near-real-time non-military GPS applications in which the cm-level accuracies required for geodesy or low-earth orbiter positioning are not essential but for which estimation speed is important. The NASA Symposium on GPS Space Applications, held in Pasadena, California, November 18–19, 1987, emphasized many of the near-real-time positioning and navigation GPS applications for spacecraft maneuvering near the Space Station and for other earth orbiters, including those at high earth altitude. Since many earth-orbiting satellites launched in the future will carry GPS equipment, including the Space Shuttle, it is likely that GPS will have an increasingly visible role in a variety of different missions. Although observing GPS from high earth altitude poses some special visibility problems, detailed analysis predicts that meter-level orbit accuracy can be achieved even for geosynchronous satellites [6].

In the future, it is expected that factorized filtering techniques will be applied to problems which would strain present computing resources to the limit. One example is recovery of gravity coefficients from GPS and low earth orbiter differential tracking data. Because there can be thousands of gravity coefficients and the data arcs required include many satellite orbit revolutions, the number of estimated parameters is expected to be in the tens of thousands [45]. Numerical stability in these situations demands extremely stable, factorized filtering algorithms. Large problems such as this one would be intractable, even on a supercomputer, were it not possible to take advantage of the local block structure in the factored covariance matrix and the fact that much of the matrix is filled with zeros [45].

V. Summary

The GPS multi-parameter estimation problem with orbit adjustment is well suited to a linearized batch sequential filter. Both the SRIF and UD-factorized filters have been used for high-accuracy GPS applications. Although neither is preferred over the other with regard to numerics, for different situations one or the other is sometimes more convenient or less expensive from a computational viewpoint. Determination of station locations to the cm level is currently feasible using GPS, with accuracy rivaling other state-of-the-art geodetic techniques. Accuracies of 1–2 parts in 10^8 relative to baseline lengths up to 2000 km have been demonstrated over baselines measured independently by radio astronomy interferometric methods, and GPS orbits determined simultaneously can now be estimated to better than 1-m accuracy. Key aspects of the estimation strategy include: collocation of three or four GPS receivers at fiducial sites with a priori, well-known coordinates; process noise modeling of fluctuating quantities such as clocks, tropospheric delays, and small but significant unmodeled satellite accelerations; multi-day orbit solutions; combined processing of pseudorange and carrier phase; and bias fixing techniques to apply integer constraints to carrier phase ambiguities. Future high-accuracy GPS applications also include sub-decimeter orbit determination for satellites such as TOPEX and Eos with non-dynamic and reduced dynamic tracking techniques, which use process noise to desensitize the filter to unmodeled or mismodeled forces.

Although considerable progress has been made in just a few years in the development of strategies for precise positioning with GPS, improvements in GPS technology promise even more gains in the near future as advanced receivers and antennas become available. Global tracking networks will greatly increase the scientific potential of GPS, and will also lead to a dramatic increase in the number of estimated state parameters. Precise pseudorange with noise of several cm will significantly advance virtually all the GPS positioning techniques developed so far. Such precise data and the anticipated filtering with very large, sparse matrices will probably require reexamination and further enhancement of the filtering approaches currently being used.

Acknowledgments

Gerald J. Bierman played a major role in developing the algorithms and filtering techniques which are discussed in this article, as can be seen from the numerous references to his work. His contributions, however, extend far beyond his analyses, algorithms, publications, and computer programs, which are recognized as the state of the art. He was a gifted yet unassuming man who shared with me his friendship as well as his extraordinary mathematical insight on the complex problems we worked on together. For me and my colleagues, his death was a great personal and professional loss.

I also thank S. C. Wu, R. P. Malla, A. P. Freedman, W. I. Bertiger, T. P. Yunck, T. Meehan, and J. T. Wu, whose work has contributed to the ideas and results presented here.

References

[1] S. M. Lichten, S. C. Wu, J. T. Wu, T. P. Yunck, "Precise Positioning Capabilities for TOPEX Using Differential GPS Techniques," AAS/AIAA Astrodynamics Specialist Conference, Vail, Colorado, paper AAS 85-401, August 12–15, 1985, published in *Astrodynamics 1985*, (ed. Kaufman et al.), vol. 58 of *Advances in the Astronautical Sciences*, pp. 597–614, 1986.

[2] "Earth Observing System: Science and Mission Requirements Working Group Report," NASA Technical Memorandum 86129, Goddard Space Flight Center, Greenbelt, Maryland, August 1984.

[3] T. P. Yunck, G. F. Lindal, and C.-H. Liu, "The Role of GPS in Precise Earth Observation," *Proceedings of the IEEE Position, Location, and Navigation Symposium*, Orlando, Florida, pp. 251–258, November 1988.

[4] A. P. Freedman and J. O. Dickey, "Usefulness of GPS for the Precise Determination of Earth Orientation Parameters," *EOS*, vol. 68, no. 44, p. 1245, November 3, 1987.

[5] S. C. Wu and R. P. Malla, "Determination of a Geocentric Coordinate Frame for GPS Measurements," *Proceedings AIAA/AAS Astrodynamics Conference*, Minneapolis, Minnesota, paper 88-4210, pp. 1–7, August 15–17, 1988.

[6] S. C. Wu, "Differential GPS Approaches to Orbit Determination of High-Altitude Earth Satellites," AAS/AIAA Astrodynamics Specialist Conference, Vail, Colorado, paper AAS 85-430, August 12–15, 1985, published in *Astrodynamics 1985*, (ed. Kaufman et al.), vol. 58 of *Advances in the Astronautical Sciences*, pp. 1203–1220, 1986.

[7] W. Melbourne, R. Anderle, M. Feissel, R. King, D. McCarthy, D. Smith, B. Tapley, and B. Vincente, "Project MERIT Standards," *United States Naval Observatory Circular No. 167*, U. S. Naval Observatory, Washington, D. C., December 27, 1983.

[8] General Dynamics, Electronics Division, *Interface Control Document 9000760*, El Segundo, California, 1976.

[9] D. A. Kerr, "Technical Operating Report for Navstar Block II Satellite," *Volume IV: Solar Force Model*, SSD81-0164-4, Rockwell International, El Segundo, California, 1982.

[10] W. Porter, *Torque Model for the GPS Space Vehicle System*, Rockwell International, El Segundo, California, 1976.

[11] O. J. Sovers, and J. S. Border, *Observational Model and Parameter Partials for the JPL Geodetic GPS Modeling Software GPSOMC*, JPL 87-21, Rev. 1, Jet Propulsion Laboratory, Pasadena, California, December 15, 1988.

[12] A. R. Thompson, J. M. Moran, and G. W. Swenson, *Interferometry and Synthesis in Radio Astronomy*, New York: John Wiley & Sons, 1986.

[13] G. E. Lanyi, "Tropospheric Delay Effects in Radio Interferometry," *TDA Progress Report 42-78*, vol. April–June 1984, Jet Propulsion Laboratory, Pasadena, California, pp. 152–159, August 15, 1984.

[14] G. J. Bierman, *Factorization Methods for Discrete Sequential Estimation*, Orlando, Florida: Academic Press, 1977.

[15] G. J. Bierman and K. H. Bierman, *Estimation Subroutine Library: Preliminary User Guide (August 1984)*, FEA Report No. 81584, Factorized Estimation Applications, Inc., Canoga Park, California, 1984.

[16] C. L. Thornton, "Triangular Covariance Factorizations for Kalman Filtering," JPL TM 33-798, Jet Propulsion Laboratory, Pasadena, California, October 1976.

[17] C. L. Thornton and G. J. Bierman, "UDU^T Covariance Factorization for Kalman Filtering," in *Control and Dynamic Systems, Advances in Theory and Application*, vol. 16, ed. C. T. Leondes, New York: Academic Press, 1980.

[18] C. L. Lawson and R. J. Hanson, *Solving Least Squares Problems*, Englewood Cliffs, New Jersey: Prentice-Hall, 1974.

[19] D. W. Allan, "Statistics of Atomic Frequency Standards," *Proc. IEEE*, vol. 54, pp. 221-230, 1966.

[20] C. L. Thornton and G. J. Bierman, "Gram-Schmidt Algorithms for Covariance Propagation," *Inst. J. Control*, vol. 25, pp. 243-260, 1977.

[21] H. E. Rauch, F. Tung, and C. T. Streibel, "Maximum Likelihood Estimates of Linear Dynamic Systems," *AIAA J.*, vol. 3, pp. 1445-1450, 1965.

[22] G. J. Bierman, "A New Computationally Efficient Fixed-Interval, Discrete-Time Smoother," *Automatica*, vol. 19, pp. 503-511, 1983.

[23] G. J. Bierman, *A Reformulation of the Rauch-Tung-Streibel Discrete Time Fixed Interval Smoother*, Bierman and Associate Report No. 870717, Studio City, California, 1987.

[24] C. L. Thornton and G. J. Bierman, "Filtering and Error Analysis Via the UDU^T Covariance Factorization," *IEEE Trans. on Automatic Control*, vol. AC-23, no. 5, pp. 901-907, 1978.

[25] G. A. Shoults, *Filtering Strategies for Non-Gravitational Accelerations With Applications to the Global Positioning System*, Masters Thesis, Purdue University, West Lafayette, Indiana, December 1987.

[26] J. M. Davidson, C. L. Thornton, S. A. Stephens, G. Blewitt, S. M. Lichten, O. J. Sovers, P. M. Kroger, L. L. Skrumeda, J. S. Border, R. E. Neilan, C. J. Vegos, B. G. Williams, J. T. Freymueller, T. H. Dixon, and W. G. Melbourne, *The Spring 1985 High Precision Baseline Test of the JPL GPS-Based Geodetic System*, JPL 87-35, Jet Propulsion Laboratory, Pasadena, California, November 15, 1987.

[27] G. Beutler, I. Bauersima, W. Gurtner, M. Rothacher, and T. Schildknecht, "Evaluation of the 1984 Alaska Global Positioning System Campaign With the Bernese GPS Software," *J. Geophys. Res.*, vol. 92, pp. 1295-1303, February 1987.

[28] R. I. Abbot, Y. Bock, C. C. Counselman III, R. W. King, S. A. Gourevitch, and B. J. Rosen, "Interferometric Determination of GPS Satellite Orbits," *Proceedings First International Symposium on Precise Positioning with GPS-1985*, ed. C. Goad, vol. I, pp. 63-72, National Geodetic Information Center, NOAA, Rockville, Maryland, 1985.

[29] R. I. Abbot, Y. Bock, C. C. Counselman, and R. W. King, "GPS Orbit Determination," *Proceedings of the Fourth International Geodetic Symposium on Satellite Positioning*, vol. I, pp. 271-274, Applied Research Laboratories, University of Texas, Austin, Texas, 1986.

[30] Y. Bock, R. I. Abbot, C. C. Counselman III, and R. W. King, "A Demonstration of 1-2 Parts in 10^7 Accuracy Using GPS," *Bull. Geod.*, vol. 60, pp. 241-254, 1986.

[31] Y. Bock, C. C. Counselman III, S. A. Gourevitch, and R. W. King, "Establishment of Three-Dimensional Control by Interferometry with the Global Positioning System," *J. Geophys. Res.*, vol. 90, pp. 7689-7703, 1985.

[32] P. L. Bender and D. R. Larden, "GPS Carrier Phase Ambiguity Resolution Over Long Baselines," *Proceedings First International Symposium on Precise Positioning with GPS-1985*, ed. C. Goad, vol. I, pp. 357-362, National Geodetic Information Center, NOAA, Rockville, Maryland, 1985.

[33] G. Blewitt, "Carrier Phase Ambiguity Resolution for the Global Positioning System Applied to Geodetic Baselines Up to 2000 km," submitted to *J. Geophys. Res.*, 1988.

[34] S. M. Lichten and J. S. Border, "Strategies For High Precision GPS Orbit Determination," *J. Geophys. Res.*, vol. 92, pp. 12751-12762, November 1987.

[35] W. I. Bertiger, S. M. Lichten, and E. C. Katsigris, "A Demonstration of Sub-Meter GPS Orbit Determination and High Precision User Positioning," *Proceedings Position, Location, and Navigation Symposium, 1988 (PLANS), IEEE*, Orlando, Florida, Nov. 29-Dec. 2, 1988.

[36] D. Dong and Y. Bock, "GPS Network Analysis: Ambiguity Resolution," *EOS*, vol. 69, no. 16, p. 325, April 1988.

[37] G. Blewitt, "Successful GPS Carrier Phase Ambiguity Resolution for Baselines up to 2000 km in Length," *EOS*, vol. 69, no. 16, p. 325, April 1988.

[38] G. H. Born, C. Wunsch, and C. A. Yamarone, "TOPEX: Observing the Oceans from Space," *EOS*, vol. 65, no. 28, pp. 433-434, July 1984.

[39] S. C. Wu, T. P. Yunck, and C. L. Thornton, "Reduced-Dynamic Technique for Precise Orbit Determination of Low Earth Satellites," paper AAS 87-410, presented at AAS/AIAA Astrodynamics Specialist Conference, Kalispell, Montana, August 10-13, 1987.

[40] J. G. Marsh et al., "A New Gravitational Model for the Earth from Satellite Tracking Data: GEM-T1," *J. Geophys. Res.*, vol. 93, pp. 6169-6215, 1988.

[41] E. R. Swift, "Comparison of GPS-Derived Earth Orientation Parameters with Final BIH/IERS Values," *EOS*, vol. 69, no. 44, p. 1154, November 1988.

[42] E. R. Swift, "NSWC's GPS Orbit/Clock Determination System," *Proceedings First International Symposium on Precise Positioning with GPS-1985*, ed. C. Goad, vol. I, pp. 51-62, National Geodetic Information Center, NOAA, Rockville, Maryland, 1985.

[43] J. M. Srinivasan et al., "Measurement of Aircraft Position, Velocity, and Orientation Using Rogue GPS Receivers: A Preliminary Report," presented at the Crustal Dynamics Project Principal Investigators' Working Group Meeting, Munich, Germany, Oct. 18-20, 1988.

[44] M. C. McIntyre, "Results of a Seafloor Positioning System Sea-Trial," *EOS*, vol. 69, no. 44, p. 1150, November 1988.

[45] S. C. Wu, J. T. Wu, and W. I. Bertiger, "An Efficient Technique for Gravity Recovery Using a Low Earth Satellite," to appear in *Proceedings of the Fifth International Symposium on Satellite Positioning*, Las Cruces, New Mexico, March 13-17, 1989.

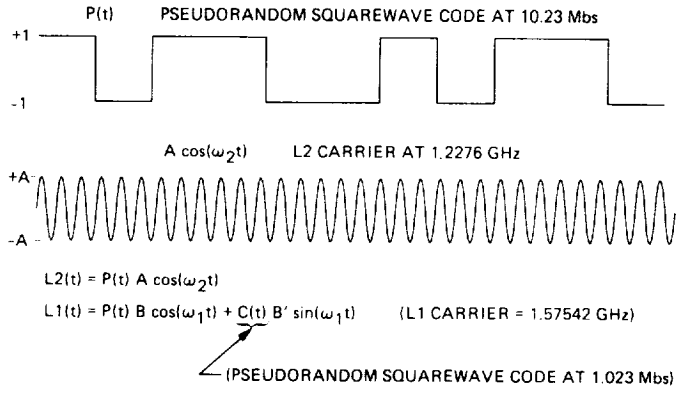

Fig. 1. GPS carrier phase is modulated by the P-code [P(t)] and the C/A code [C(t)]. The P-code contains nominal values for GPS orbits and clocks. Carrier phase and P-code pseudorange are used in high-accuracy applications.

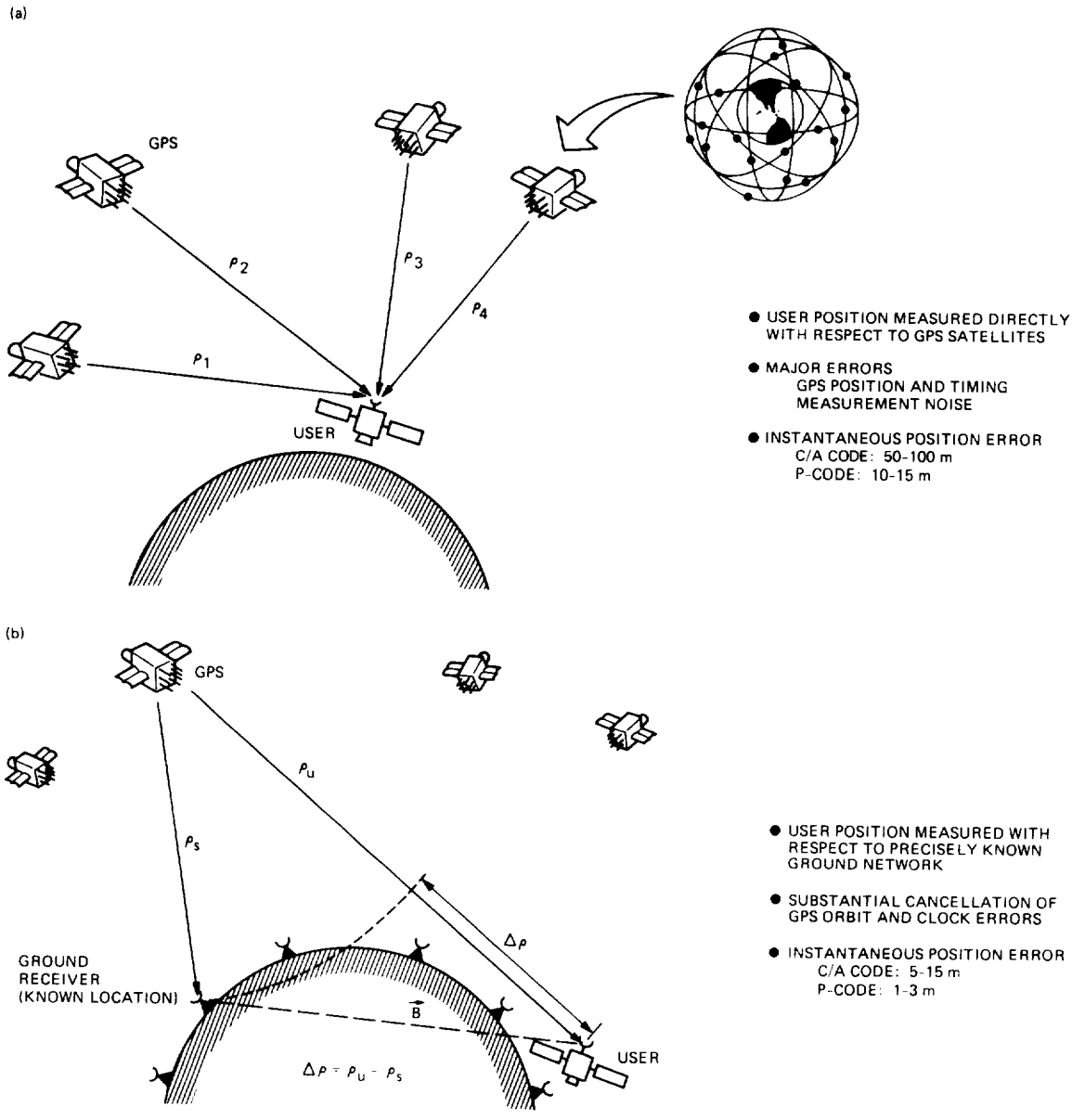

Fig. 2. (a) Direct GPS tracking, and (b) differential GPS tracking.

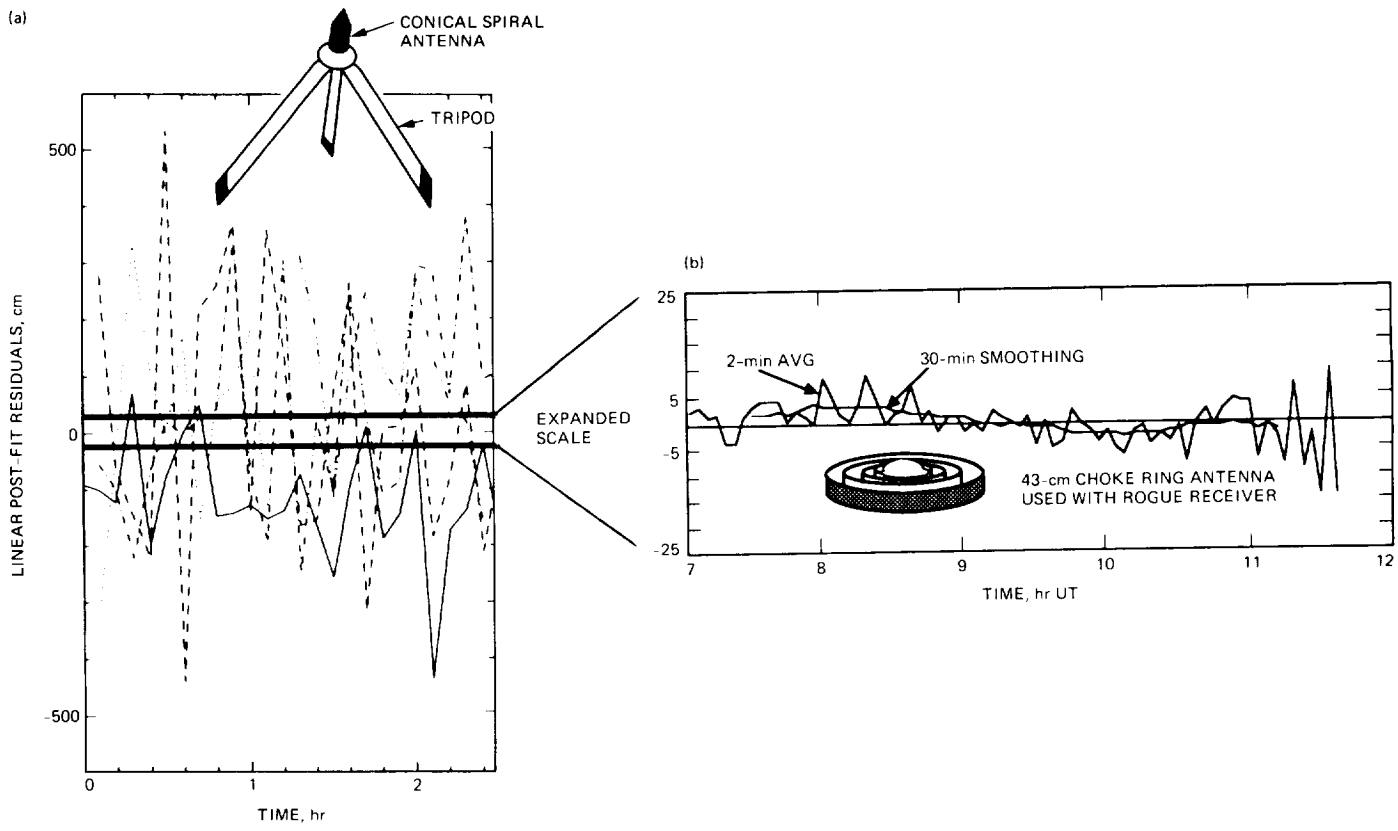

Fig. 3. Comparison between performance with different antenna and receiver designs: (a) post-fit residuals, mostly multipath, for dual-frequency pseudorange averaged over six minutes from a common TI antenna/receiver combination, and (b) pseudorange scatter obtained in January 1988 with the JPL Rogue receiver and a choke ring antenna designed to minimize multipath, for single-frequency data averaged over 2- and 30-minute intervals.

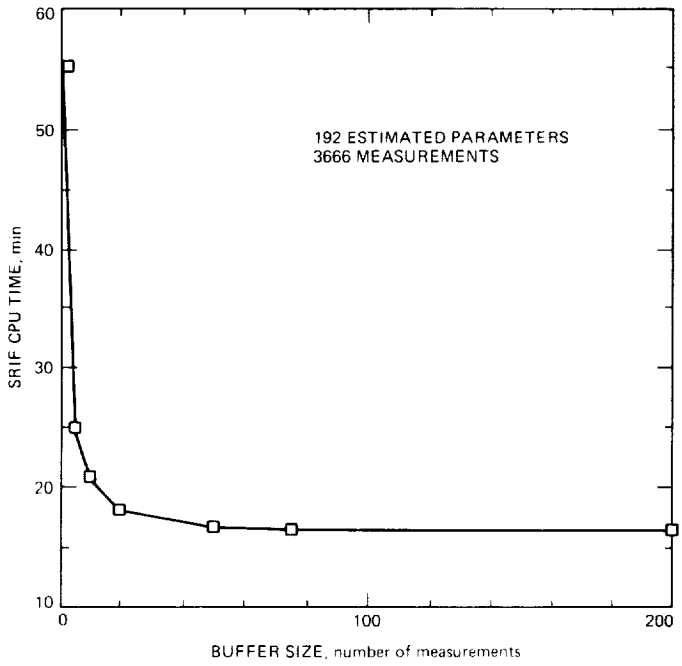

Fig. 4. Comparison of CPU time required for the SRIF for different measurement buffer sizes.

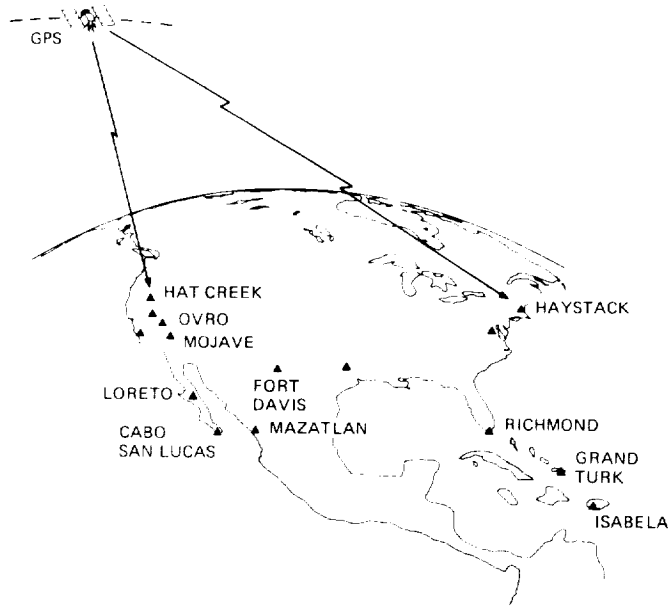

Fig. 5. Locations of ground receivers during 1985 and 1986 GPS experiments.

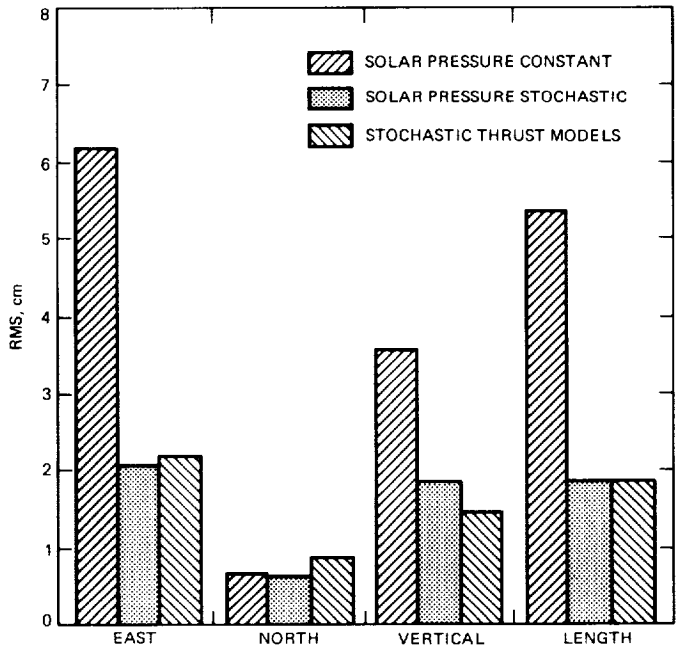

Fig. 6. Daily repeatability for the 1314-km Mojave, California – Fort Davis, Texas baseline, for a two-week data arc in November, 1985. Lowest scatter is obtained with process noise force models.

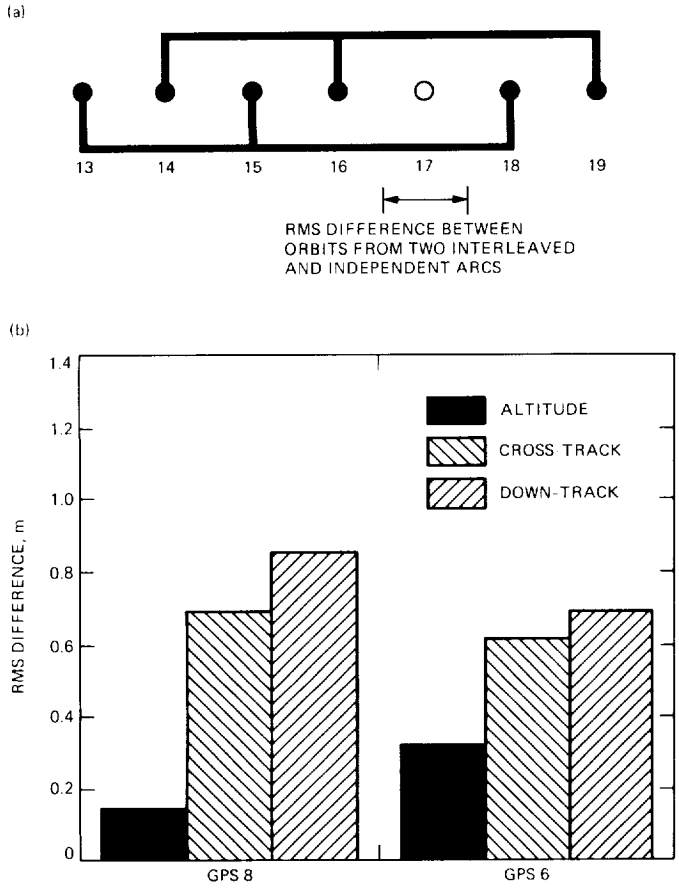

Fig. 7. (a) RMS orbit difference is computed from interleaved orbits determined independently from November 13–15–18 and November 14–16–19; (b) RMS for GPS 6 and GPS 8 is shown computed over a 24-hour period on November 17 when no measurements were used for either solution as shown in (a).

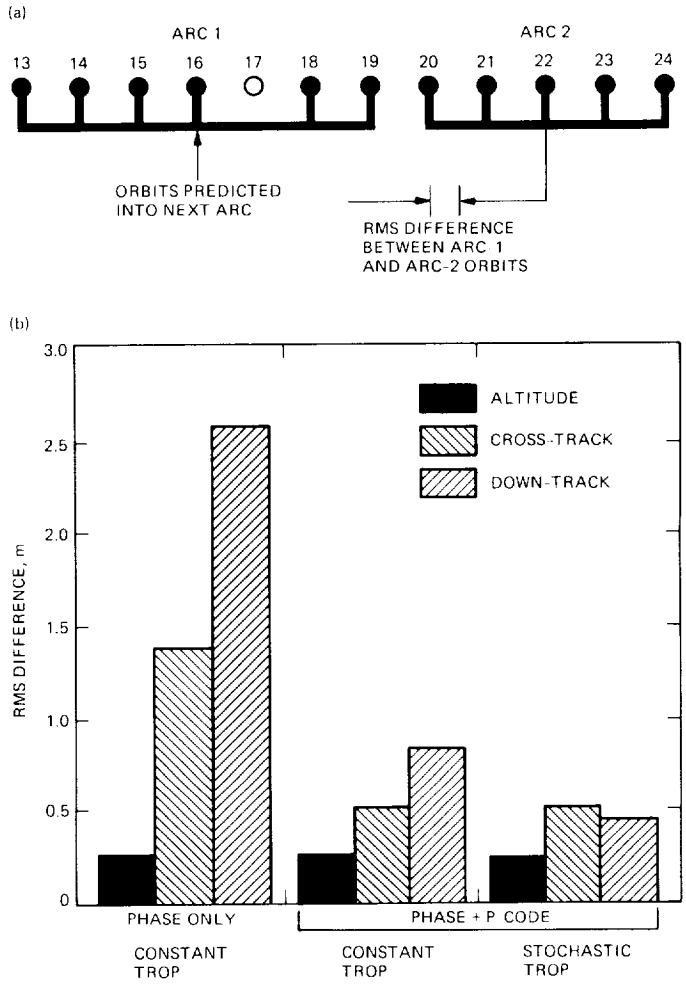

Fig. 8. (a) One week arcs in November 1985 used for orbit prediction and RMS computation. Orbits from the first week are mapped ahead and compared to orbits determined independently using data only from the second week; (b) prediction test (Fig. 8a) for GPS 8 shows RMS well below 1 meter in all three components, with best results obtained using stochastic troposphere models and combined carrier phase and P-code pseudorange. RMS is computed over a 6-hour interval.

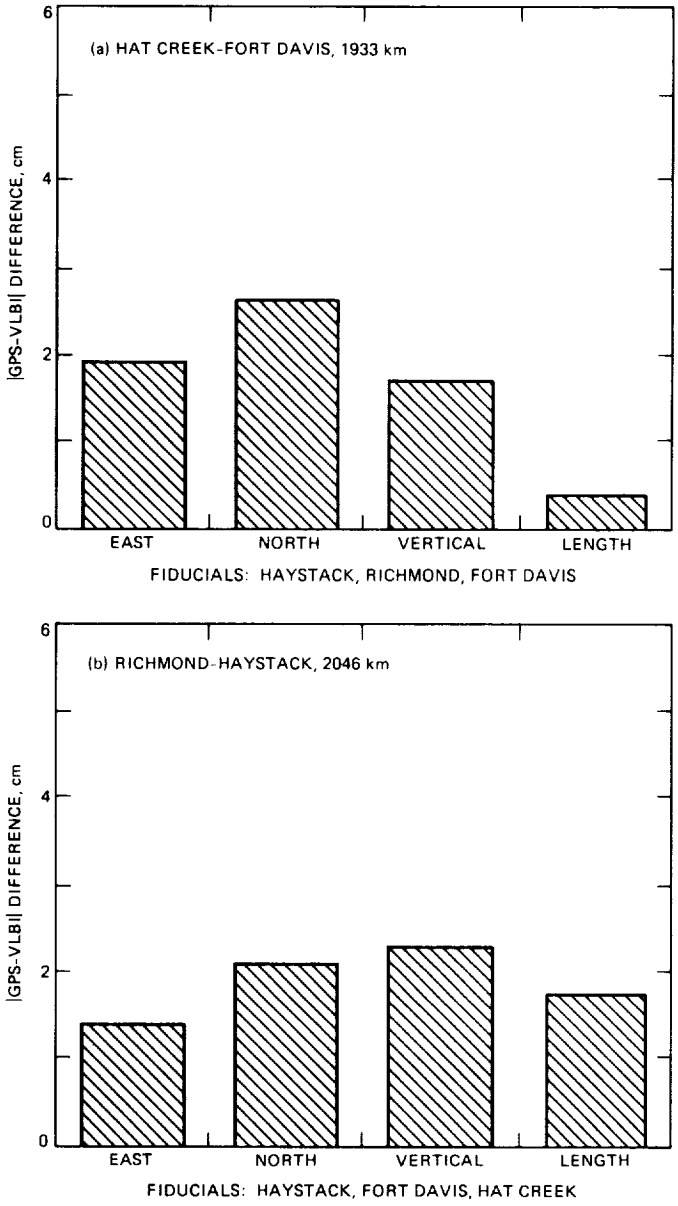

Fig. 9. Comparison between GPS and VLBI independent measurements of 2000-km baselines shows agreement of 1–2 parts in 10^8 in all vector components: (a) Hat Creek–Fort Davis, and (b) Richmond–Haystack.

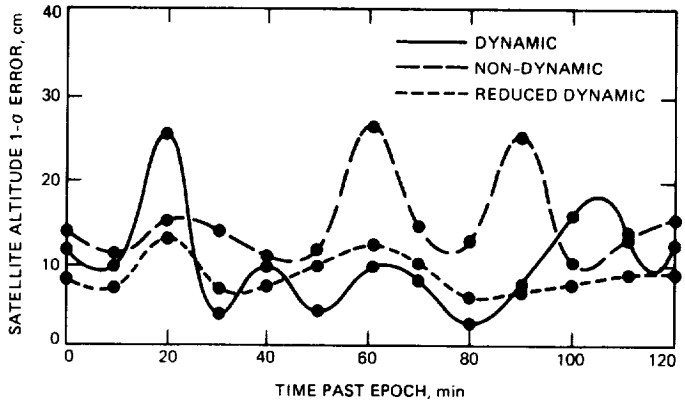

Fig. 10. Predicted altitude accuracy for TOPEX orbit determination using dynamic, reduced dynamic, and non-dynamic tracking techniques.